analytical chemistry

Article

Cite This: Anal. Chem. 2019, 91, 5747−5752

pubs.acs.org/ac

Direct Observation of Nanoparticles within Cells at Subcellular Levels by Super-Resolution Fluorescence Imaging

Shasha Chen,[†,§] Jie Wang,[†,§] Bo Xin,[‡] Yanbing Yang,[†] Yurou Ma,[†] Yu Zhou,[†] Liangjie Yuan,[†] Zhenli Huang,*[,‡] and Quan Yuan*[,†]

[†]Key Laboratory of Analytical Chemistry for Biology and Medicine (Ministry of Education), College of Chemistry and Molecular Sciences, Wuhan University, Wuhan 430072, PR China

[‡]Wuhan National Laboratory for Optoelectronics, Huazhong University of Science and Technology, Wuhan 430074, PR China

Supporting Information

ABSTRACT: Direct observation of nanoparticles with high spatial resolution at subcellular levels is of great importance to understand the nanotoxicology and promote the biomedical applications of nanoparticles. Super-resolution fluorescence microscopy can break the diffraction resolution limit to achieve spatial resolution of tens of nanometers, making it ideal for highly accurate observation of nanoparticles in the cellular world. In this study, we introduced the employment of super-resolution fluorescence imaging for monitoring nanoparticles within cells. Carbocyanine dyes Alexa Flour 647 labeled mesoporous silica nanoparticles (designated as MSNs-AF647) were constructed as the super-resolution imaging nanoplatform in this work as proof of concept. The MSNs-AF647 were incubated with Hela cells, and the nanoparticles within cells were further monitored by super-resolution fluorescence microscopy. The fluorescence images of MSNs-AF647 within cells captured with the super-resolution fluorescence microscopy showed a much higher spatial resolution than that obtained using conventional fluorescence microscopy, showing that super-resolution fluorescence images can provide more accurate information to locate the nanoparticles at the subcellular levels. Moreover, other functional molecules can be easily loaded into the MSNs-AF647 super-resolution imaging nanoplatform, which suggested that super-resolution fluorescence imaging can further be applied to various bioimaging-related areas, such as imaging-guided therapy, with the aid of the MSNs-AF647 nanoplatform. This study demonstrates that super-resolution fluorescence microscopy offers a highly accurate method to study nanoparticles in the cellular world. We anticipate this strategy may further be applied to research areas such as studying the nanotoxicology and optimization of nanoparticle-based bioprobes or drugs by designing new nanostructured materials with multifunctional properties based on MSNs-AF647.

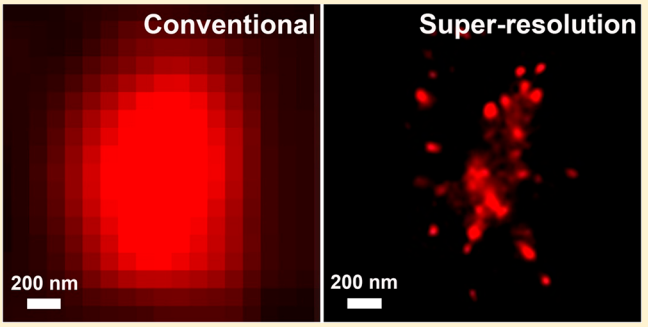

Nanoparticles, such as mesoporous silica nanoparticles (MSNs), carbon nanotubes, liposomes, fluorescent quantum dots, gold nanorods, superparamagnetic nanoparticles, etc., are widely used in biosensing, bioimaging, and cancer therapy.[1] Studying the behaviors of nanoparticles in the cellular world can provide important information for optimizing their biomedical performance.[2−8] To date, research on nanoparticles within cells are usually carried out either by conventional fluorescence microscopy or by electron microscopy.[9−13] Fluorescence microscopy can observe specific cell components or cellular events, and it has been widely used in noninvasive and real-time bioimaging.[14−16] In spite of such advantages, fluorescence microscopy cannot reveal detailed structural organization of biomolecules or subcellular organelles because the diffraction of light limits the spatial resolution of conventional fluorescence microscopy to about 200−300 nm in the lateral direction and 500−700 nm in the axial direction.[17] As for electron microscopy, the resolution can reach nanometers, but the disadvantages such as invasiveness, complicated sample preparation, and expensive instrumentation significantly limit its biomedical application.[18,19] Therefore, there is still an urgent need to develop an easy-to-perform method with high spatial resolution to study the behaviors of nanoparticles in the cellular world.

Compared with conventional fluorescence microscopy, the spatial resolution of super-resolution fluorescence microscopy can reach down to tens of nanometers by overcoming the diffraction resolution limit, which makes super-resolution fluorescence microscopy ideal for bioimaging at the subcellular or even single molecular levels.[20−29] Generally, super-resolution fluorescence microscopy techniques include stimulated emission depletion (STED) microscopy,[20−23] stochastic optical reconstruction microscopy (STORM),[24−27] photoactivated localization microscopy (PALM),[28,29] and so on. As

Received: December 24, 2018
Accepted: April 2, 2019
Published: April 2, 2019

DOI: 10.1021/acs.analchem.8b05919
Anal. Chem. 2019, 91, 5747−5752

one of the most popular techniques, STORM is based on the detection and localization of a single fluorescent molecule, which makes the lateral resolution of STORM down to 20−30 nm.[24,30] In the past years, STORM has been widely used in cell biology,[31] such as discriminating the nanoscale structures of cell organelles[32,33] and exploring the biodistributions of proteins on cell membranes.[34,35] Recently, the application of STORM in material science has been reported. Zhu et al. used super-resolution fluorescence microscopy to monitor the self-assembly of block copolymers.[36] Li et al. employed STORM to observe the distribution of gelatin in crystalline polymorphs of calcium carbonate crystals.[37] In spite of such achievements, there are few reports about the applications of super-resolution fluorescence microscopy in studying nanoparticles in the cellular world.

The MSNs are one of the most widely used nanoparticles in controlled drug delivery,[38−40] biosensing,[41,42] gene transport/expression,[43−45] and biolabeling.[46] Herein, by using MSNs as the model, we demonstrated the potent ability of STORM in monitoring nanoparticles within cells by construction of carbocyanine dye Alexa Flour 647 labeled MSNs (designated as MSNs-AF647) as a proof of concept. Results demonstrated that the super-resolution fluorescence images of MSNs-AF647 displayed a much higher spatial resolution than conventional fluorescence images. The MSNs-AF647 in Hela cells can be clearly observed with high accuracy by the super-resolution fluorescence microcopy. More importantly, the MSNs-AF647 super-resolution imaging nanoplatform can be loaded with other functional molecules for various potential biomedical applications. The developed strategy may further contribute to the study of the nanotoxicology and provide valuable information for nanomaterials-based biosensing, bioimaging, or cancer therapy through the engineering of multifunctional novel nanomaterials with MSNs-AF647.

EXPERIMENTAL DETAILS

Materials and Reagents. Tetraethylorthosilicate (TEOS) (≥28.4%), *N*-cetyltrimethylammonium bromide (CTAB) (≥99.0%), sodium hydroxide (≥96.0%), methanol (≥99.5%), hydrochloric acid (∼36.0−38.0%), toluene (≥99.5%), sodium bicarbonate (≥99.5%), and fluorescein were purchased from Sinopharm Chemical Reagent Co., Ltd. The 3-aminopropyltriethoxysilane (APTES) (≥99.0%) and dimethyl sulfoxide (DMSO) (≥99.9%) were purchased from Aladin. Alexa Flour 647 was obtained from Thermo Fisher Scientific Inc. Deionized (DI) water (resistivity ∼18.25 MΩ) was used for all experiments.

Sample Characterization. Transmission electron microscopy (TEM) images were recorded by a JEM-2100 transmission electron microscope (JEOL) with an accelerating voltage of 200 kV. Zeta potential measurements were conducted using a Malvern Zetasizer Nano ZS system. The phase of nanocrystals was carried out using a Bruker D8 Advance X-ray diffractometer with a Cu−Kα radiation (λ = 1.5406 Å). Luminescence spectra was recorded on a Hitachi F-4600 fluorescence spectrometer. The N_2 adsorption and desorption isotherms were measured at 77 K using an ASAP 2010 analyzer (Micromeritics). FT-IR spectra were recorded by Fourier transform infrared spectroscopy (Nicolet 5700) from 4000 to 400^{-1}. Confocal microscopy images were taken by Zeiss LMS710 XD with a 63×/1.46-NA oil-immersion objective. Super-resolution fluorescence images were taken by a sCMOS camera (Flash 4.0, Hamamatsu Photonics) with a 100×/1.4-NA oil-immersion objective.

Synthesis of Alexa Flour 647 Labeled Mesoporous Silica Nanoparticles (MSNs-AF647). MSNs were prepared by a base-catalyzed sol−gel procedure according to previous literature.[47] Briefly, CTAB (250 mg) was initially dissolved in 120 mL of distilled water, and then 0.875 mL of NaOH solution (2 M) was slowly added to CTAB solution under vigorous stirring. Subsequently, the reaction was performed at 80 °C for 30 min. Afterward, TEOS (1.25 mL) was added dropwise to the above solution, and the mixture was vigorously stirred for 2 h until white precipitates were obtained. After cooling to room temperature, the obtained product was centrifuged and washed with distilled water and methanol. The product was further dried at room temperature under vacuum. To remove the surfactant template (CTAB), the as-synthesized solid product was refluxed at 80 °C for 24 h in a mixture of HCl (9 mL) and methanol (200 mL). Then, MSNs with uniform meso-structural were obtained after washing with distilled water and methanol. The as prepared MSNs were dried at room temperature under vacuum. The MSN-NH_2 was synthesized by the following procedures. Typically, 50 mg of dried MSNs was suspended in 20 mL of toluene, and then 30 μL of APTES was added into the above solution. The mixture was stirred at room temperature for 20 h and then evaporated by a rotary evaporator to obtain MSN-NH_2. For synthesizing MSNs-AF647, 20 mg of MSNs-NH_2 was suspended in 5 mL of 0.2 M $NaHCO_3$ solution, then 5 μL of AF647 in DMSO (0.4 g/L) was added and stirred at room temperature for 3 h. After that, the particles were centrifuged and washed with distilled water many times, Then the obtained MSNs-AF647 was dried at room temperature under vacuum.

Synthesis of MSNs-AF647/Fluorescein and MSNs/Fluorescein. The obtained MSNs-AF647 were suspended in 5 mL of distilled water, and then 10 mL of fluorescein (1 mM) was added into the above dispersions under vigorous stirring. The mixture was allowed to react for 12 h at room temperature. The MSNs-AF647/fluorescein was obtained after centrifuging and washing the products with distilled water three times. Then the obtained MSNs-AF647/fluorescein was dried at room temperature under vacuum. The preparation of MSNs/fluorescein was similar to the preparation of MSNs-AF647/fluorescein by replacing MSNs-AF647 with MSNs.

Cellular Uptake of MSNs-AF647. Hela cells were grown in Dulbecco's Modified Eagle Medium (DMEM, Gibco) supplemented with 10% fetal bovine serum (FBS, Gibco) and 1% penicillin (10 000 IU/mL)/streptomycin (10 000 μg/mL) at 37 °C with 5% CO_2. Before imaging, cells were seeded on 35 mm glass-bottom dishes overnight and then treated with 100 μg/mL of MSNs-AF647 for 5 h. For super-resolution imaging, the cells were washed with PBS three times, fixed with 4% paraformaldehyde (PFA), and washed with PBS three times again. Cells soaked with imaging buffer[48] were imaged under a custom-built super-resolution microscope.

Intracellular Location. To determine the intracellular location of MSNs-AF647, the cells treated with MSNs-AF647 were incubated with 100 nM LysoTracker Green DND-26 for 45 min. Images were recorded on a confocal microscope with a 60×/1.42-NA oil-immersion objective. LysoTracker Green and MSNs-AF647 were activated at wavelengths of 488 and 640 nm, respectively.

DOI: 10.1021/acs.analchem.8b05919
Anal. Chem. 2019, 91, 5747−5752

Super-Resolution Fluorescence Imaging of MSNs-AF647. The super-resolution experiments were performed on an Olympus IX71 inverted optical microscope. The 640 and 405 nm laser lines were combined and coupled into an optical fiber, and the fiber output was collimated and focused on the back focal plane of a high-numerical-aperture (NA) oil-immersion objective (100×, NA1.4; Olympus). Samples of MSNs-AF647 soaked with imaging buffer were imaged with the 640 nm laser at an intensity of 6 kW cm^{-2}. During imaging, the intensity of the 405 nm activation laser was manually increased to make a suitable blinking density. A series of 10 000 images was captured with a sCMOS camera (Flash 4.0, Hamamatsu Photonics) at a frame rate of 50 Hz (exposure time, 20 ms) and the pixel size was 100 nm. All the images were analyzed by MaLiang[49] (an ImageJ plug-in written in Java).

RESULTS AND DISCUSSION

The schematic illustration of the preparation of MSNs-AF647 super-resolution imaging nanoplatform is shown in Scheme 1a.

Scheme 1. (a) Schematic Illustration of the Preparation of MSNs-AF647 Super-Resolution Imaging Nanoplatform, (b) Conventional Fluorescence Image (Left) and Super-Resolution Fluorescence Image (Right) of MSNs-AF647, and (c) Schematic Illustration of the Super-Resolution Fluorescence Imaging of MSNs-AF647

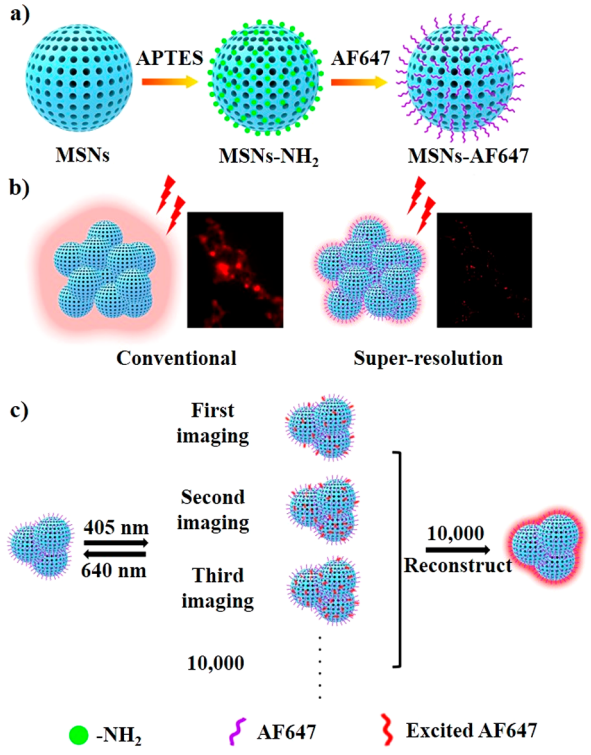

The MSNs are functionalized with amine groups (MSNs-NH_2) by the hydrolysis of 3-aminopropyl triethoxysilane (APTES) on their surfaces. The MSNs-NH_2 further react with the carboxylic acid groups of AF647 to obtain MSNs-AF647 through the formation of an amide bond. Conventional fluorescent image and the super-resolution fluorescent image of MSNs-AF647 are shown in Scheme 1b. The super-resolution fluorescence image of the MSNs-AF647 obtained with STORM shows a much higher spatial resolution than the conventional fluorescence image. The mechanism under the high resolution is illustrated in Scheme 1c. The super-resolution fluorescence image achieved by STORM is a reconstructed image which is reconstructed with 10 000 fluorescence images. Each fluorescence image is observed according to the following processes. First, all the AF647 molecules are bleached at the excitation wavelength of 640 nm with higher power. Then, the sparse subset of AF647 molecules is activated at the excitation wavelength of 405 nm and imaged until they are bleached at the excitation wavelength of 640 nm. During this process, each molecule is localized with high precision and the location of each molecule is recorded by computer to obtain one fluorescence image. By sequentially activating sparse subsets of AF647 molecules on the nanoparticles, imaging the AF647 until they are bleached, and localizing each molecule with high precision, 10 000 fluorescence images are collected. These 10 000 fluorescence images are further reconstructed by algorithmic processing to obtain the precise location of the MSNs-AF647.

The structures of the MSNs-AF647 were systematically characterized. TEM images indicate that the MSNs-AF647 show the hexagonal arranged moso-structure and are well-dispersed with uniform shape and size (Figure 1a, Figure S5).

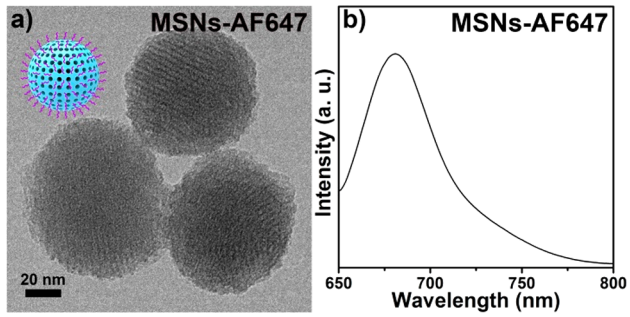

Figure 1. (a) TEM image of MSNs-AF647 and (b) photoluminescence spectra of MSNs-AF647.

The average diameter of MSNs-AF647 is determined to be about 80 nm. The ordered moso-structure is also clearly evidenced by the small-angle X-ray diffraction (SAXRD) pattern (Figure S6). Figure 1b shows that the MSNs-AF647 displays the typical emission band of AF647 at about 680 nm, suggesting the successful conjugation of AF647 to the MSNs.

The ability of STORM in improving spatial resolution for locating MSNs-AF647 was further investigated. Fluorescent images of the MSNs-AF647 were captured with conventional fluorescence microscopy and super-resolution fluorescence microscopy, respectively. As shown in Figure 2a, the image of MSNs-AF647 captured with conventional fluorescence microscopy exhibits large fluorescence domains with diameters in the range of several micrometers. In contrast, the super-resolution fluorescence image of MSNs-AF647 in the same area (Figure 2b) shows clear and much smaller fluorescence spots. The sizes of the small subdomains within the fluorescence spots are in the nanometers range, much smaller than the fluorescence domains in image obtained with the conventional fluorescence microscopy. Fluorescent images captured with the conventional fluorescence microscopy and super-resolution fluorescence microscopy were further progressively zoomed (Figure S8). Significantly improved spatial resolution can be observed in super-resolution fluorescence

DOI: 10.1021/acs.analchem.8b05919
Anal. Chem. 2019, 91, 5747−5752

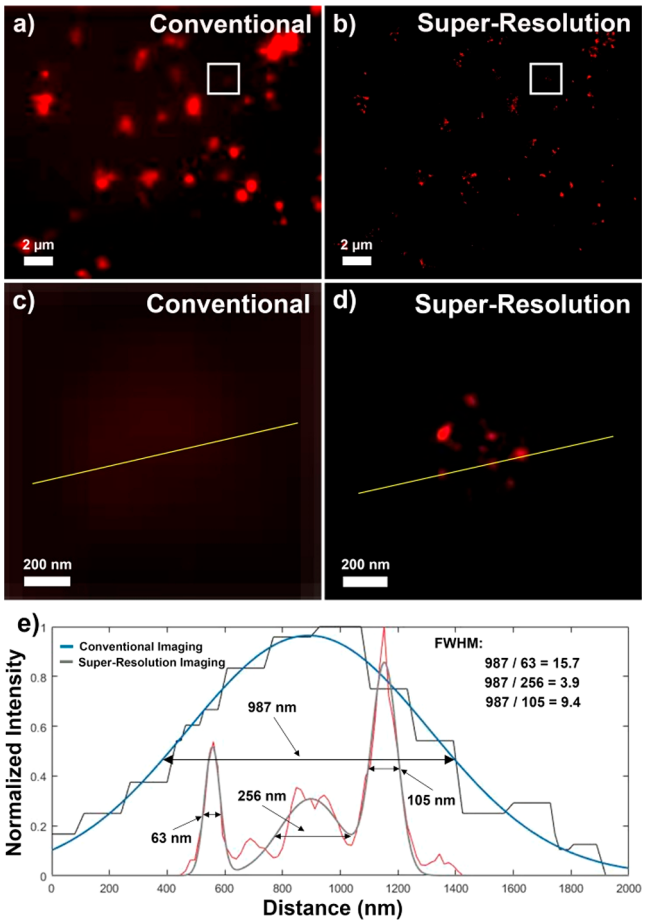

Figure 2. Conventional (a) and super-resolution (b) fluorescence images of MSNs-AF647. (c) High magnification image of the white dashed box in part a. (d) High-magnification image of the white dashed box in part b. (e) Fluorescence cross-sectional profiles for the determination of fwhm.

images. To further show the improved spatial resolution by super-resolution fluorescence imaging, the full-width at half-maximum (fwhm) of the localized fluorescent nanoparticles was measured (Figure 2c–e). For the conventional fluorescence image, the fwhm of the localized fluorescent domain is determined to be 987 nm with Gaussian deconvolution. In the same area of the super-resolution fluorescence image, three fluorescence spots are clearly observed. The fwhm of the three spots are calculated to be 63, 256, and 105 nm from Gaussian deconvolution, respectively, which clearly shows an obvious enhancement in resolution by super-resolution fluorescence microscopy. The above results clearly indicate that super-resolution fluorescence imaging can locate the position of MSNs-AF647 with high spatial resolution.

The MSNs-AF647 super-resolution imaging nanoplatform were further incubated with Hela cells, and the MSNs-AF647 within cells were directly observed with STORM (Figure 3a). Co-localization tests show that the MSNs-AF647 are mainly accumulated in the endosomes and lysosomes of the Hela cells (Figure S9). Similarly, the fluorescence images of the endocytosed MSNs-AF647 were captured with conventional fluorescence microscopy and super-resolution fluorescence microscopy, respectively. As shown in Figure 3b, the conventional fluorescence image indicates that the MSNs-AF647 are spread over the cytoplasm of Hela cells in the form

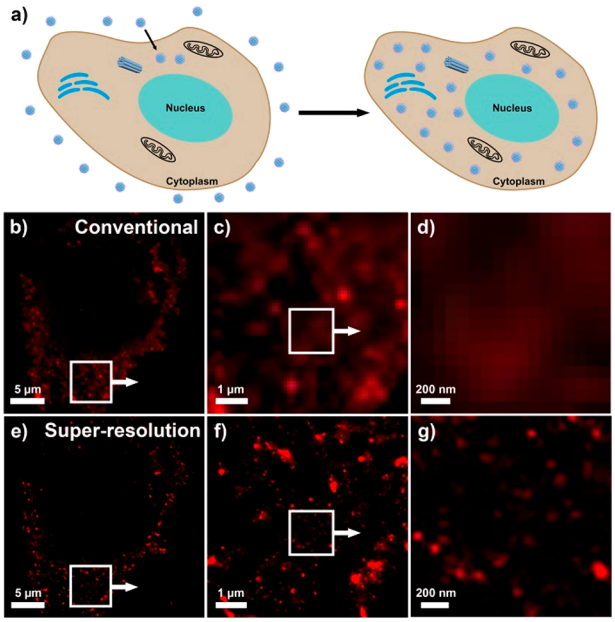

Figure 3. (a) Schematic illustration of incubating MSNs-AF647 with Hela cells. (b–d) Progressively zoomed-in conventional fluorescence images of MSNs-AF647 within a single cell. (e–g) Progressively zoomed-in super-resolution fluorescence images of MSNs-AF647 within a single cell.

of large microdomains. At higher magnifications (Figure 3c,d), the microdomains become blurry and the location of MSNs-AF647 cannot be discriminated. However, for the same area on the image captured by super-resolution fluorescence microscopy (Figure 3e), a remarkable increase in spatial resolution is observed. The MSNs-AF647 exhibit clear fluorescence spots that are composed of many small subdomains with sizes in the nanometer range (Figure 3f,g). These results clearly indicate the good potential of super-resolution fluorescence microscopy in locating nanoparticles in cells with high spatial resolution.

The MSNs-AF647 super-resolution imaging nanoplatform can further be used in designing multifunctional bioprobes for bioimaging-related applications. As proof of concept, fluorescein was employed as a model for functional molecules and was loaded into the MSNs-AF647 (designated as MSNs-AF647/fluorescein). The MSNs-AF647/fluorescein multifunctional bioprobe was characterized with confocal microscopy. As shown in Figure 4, strong green fluorescence from fluorescein (Figure 4b) and red fluorescence from AF647 (Figure 4c) are clearly observed. The red fluorescence of AF647 colocalizes with the green fluorescence of fluorescein (Figure 4d). By simply replacing the fluorescein by functional molecules such as doxorubicin, the MSNs-AF647 can further be used in super-resolution imaging guided therapy to study the pharmacokinetics and optimize the therapy efficiency of the nanoparticle-based drugs. These results suggest the great potential of the MSNs-AF647 super-resolution imaging nanoplatform in promoting the biomedical applications of nanoparticles.

CONCLUSION

In conclusion, we reported the employment of super-resolution fluorescence microcopy to observe nanoparticles within cells with high spatial resolution. The MSNs-AF647 conjugates were designed as a super-resolution imaging nanoplatform, and

DOI: 10.1021/acs.analchem.8b05919
Anal. Chem. 2019, 91, 5747–5752

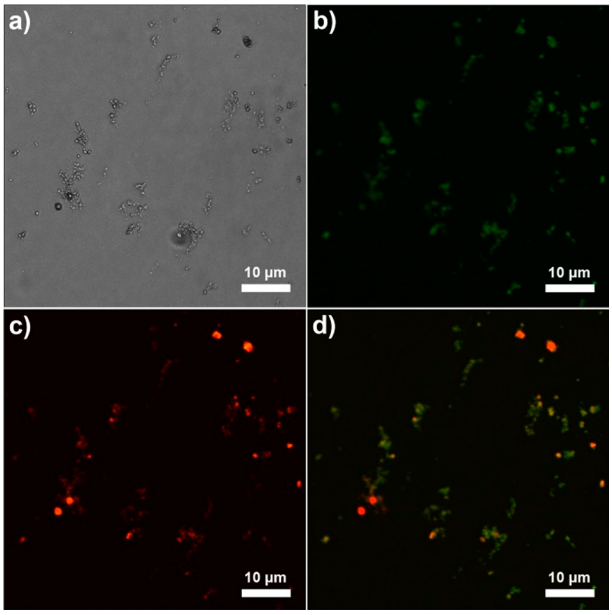

Figure 4. (a) Bright field of MSNs-AF647/fluorescein, (b) green fluorescence from fluorescein, (c) red fluorescence from AF647, and (d) merged image of parts b and c.

the nanoplatforms in the cells were directly monitored with STORM. The super-resolution fluorescence microscopy exhibits a much higher spatial resolution than the conventional fluorescence microscopy in locating the MSNs-AF647 within cells. Moreover, the MSNs-AF647 super-resolution imaging nanoplatform can further be employed to design multifunctional bioprobes for super-resolution bioimaging or super-resolution imaging guided therapy. The strategy developed in our study may open up new opportunities in areas such as studying the nanotoxicology and optimization of nanoparticle-based anticancer drugs.

■ ASSOCIATED CONTENT

Supporting Information

The Supporting Information is available free of charge on the ACS Publications Web site. The Supporting Information is available free of charge on the ACS Publications website at DOI: 10.1021/acs.analchem.8b05919.

TEM images of MSNs (Figure S1); nitrogen adsorption−desorption isotherms of MSNs (Figure S2); TEM images of MSNs-NH_2 (Figure S3); zeta potentials of MSN and MSN-NH_2 (Figure S4); TEM images of MSNs-AF647 (Figure S5); SAXRD diffraction pattern of MSNs, MSNs-NH_2, and MSNs-AF647 (Figure S6); FT-IR spectra of MSNs and MSNs-AF647 (Figure S7); progressively zoomed-in fluorescence images (Figure S8); confocal microscopic images of Hela cells incubated with MSNs-AF647 (Figure S9); and progressively zoomed-in fluorescence images of MSNs-AF647 within a single cell (Figure S10) (PDF)

■ AUTHOR INFORMATION

Corresponding Authors

*E-mail: yuanquan@whu.edu.cn.
*E-mail: leo@mail.hust.edu.cn.

ORCID

Jie Wang: 0000-0003-4170-8470
Liangjie Yuan: 0000-0002-6862-7569
Quan Yuan: 0000-0002-3085-431X

Author Contributions

§S.C. and J.W. contributed equally to this work.

Notes

The authors declare no competing financial interest.

■ ACKNOWLEDGMENTS

This work was supported by the National Key Research and Development Program of China (2017YFA0208000), National Natural Science Foundation of China (21675120), and The Foundation for Innovative Research Groups of NSFC (21521063). Q. Yuan thanks the large-scale instrument and equipment sharing foundation of Wuhan University.

■ REFERENCES

(1) He, Q.; Zhang, Z.; Gao, F.; Li, Y.; Shi, J. *Small* **2011**, *7*, 271−280.
(2) Joseph, M. M.; Nair, J. B.; Maiti, K. K.; Therakathinal, T. S. *Biomacromolecules* **2017**, *18*, 4041−4053.
(3) Lee, Y. K.; Kim, S.-W.; Park, J.-Y.; Kang, W. C.; Kang, Y. J.; Khang, D. *Int. J. Nanomed.* **2017**, *12*, 5761−5779.
(4) Yaghini, E.; Turner, H. D.; Le Marois, A. M.; Suhling, K.; Naasani, I.; MacRobert, A. J. *Biomaterials* **2016**, *104*, 182−191.
(5) Carregal-Romero, S.; Plaza-Garcia, S.; Pinol, R.; Murillo, J.; Ruiz-Cabello, J.; Padro, D.; Millan, A.; Ramos-Cabrer, P. *Biosensors* **2018**, *8*, 127.
(6) Yingyuad, P.; Sinthuvanich, C.; Leepasert, T.; Thongyoo, P.; Boonrungsiman, S. *J. Drug Delivery Sci. Technol.* **2018**, *44*, 491−497.
(7) Iannarelli, L.; Giovannozzi, A. M.; Morelli, F.; Viscotti, F.; Bigini, P.; Maurino, V.; Spoto, G.; Martra, G.; Ortel, E.; Hodoroaba, V.-D.; Rossi, A. M.; Diomede, L. *RSC Adv.* **2016**, *6*, 70501−70509.
(8) Xu, X.; Wu, C.; Bai, A.; Liu, X.; Lv, H.; Liu, Y. *J. Nanomater.* **2017**, *2017*, 1−13.
(9) Doh, J. K.; White, J. D.; Zane, H. K.; Chang, Y. H.; López, C. S.; Enns, C. A.; Beatty, K. E. *Proc. Natl. Acad. Sci. U. S. A.* **2018**, *115*, 12961−12966.
(10) Gao, H.; Yang, Z.; Zhang, S.; Cao, S.; Shen, S.; Pang, Z.; Jiang, X. *Sci. Rep.* **2013**, *3*, 2534.
(11) Song, R.; Shi, Q.; Abdrabboh, G. A.; Wei, R. *Process Biochem.* **2017**, *62*, 223−230.
(12) Ali, M. R.; Panikkanvalappil, S. R.; El-Sayed, M. A. *J. Am. Chem. Soc.* **2014**, *136*, 4464−4467.
(13) Kim, E. B.; Seo, J. M.; Kim, G. W.; Lee, S. Y.; Park, T. J. *Enzyme Microb. Technol.* **2016**, *95*, 201−208.
(14) Sokolova, V.; Shi, Z.; Huang, S.; Du, Y.; Kopp, M.; Frede, A.; Knuschke, T.; Buer, J.; Yang, D.; Wu, J.; Westendorf, A. M.; Epple, M. *Acta Biomater.* **2017**, *64*, 401−410.
(15) Leung, C. W.; Hong, Y.; Chen, S.; Zhao, E.; Lam, J. W.; Tang, B. Z. *J. Am. Chem. Soc.* **2013**, *135*, 62−65.
(16) Chen, S.; Hong, Y.; Liu, Y.; Liu, J.; Leung, C. W.; Li, M.; Kwok, R. T.; Zhao, E.; Lam, J. W.; Yu, Y.; Tang, B. Z. *J. Am. Chem. Soc.* **2013**, *135*, 4926−4929.
(17) Bates, M.; Huang, B.; Zhuang, X. *Curr. Opin. Chem. Biol.* **2008**, *12*, 505−514.
(18) Dahmke, I. N.; Verch, A.; Hermannsdörfer, J.; Peckys, D. B.; Weatherup, R. S.; Hofmann, S.; de Jonge, N. *ACS Nano* **2017**, *11*, 11108−11117.
(19) Huang, B.; Bates, M.; Zhuang, X. *Annu. Rev. Biochem.* **2009**, *78*, 993−1016.
(20) Müller, T.; Schumann, C.; Kraegeloh, A. *ChemPhysChem* **2012**, *13*, 1986−2000.
(21) Jin, D.; Xi, P.; Wang, B.; Zhang, L.; Enderlein, J.; van Oijen, A. M. *Nat. Methods* **2018**, *15*, 415−423.
(22) Tavernaro, I.; Cavelius, C.; Peuschel, H.; Kraegeloh, A. *Beilstein J. Nanotechnol.* **2017**, *8*, 1283−1296.

DOI: 10.1021/acs.analchem.8b05919
Anal. Chem. 2019, 91, 5747−5752

(23) Shin, K.; Jung, T.; Lee, E.; Lee, G.; Goh, Y.; Heo, J.; Jung, M.; Jo, E.-J.; Lee, H.; Kim, M.-G.; Lee, K. T. *Phys. Chem. Chem. Phys.* **2017**, *19*, 9739−9744.
(24) Rust, M. J.; Bates, M.; Zhuang, X. *Nat. Methods* **2006**, *3*, 793−795.
(25) Valiya Peedikakkal, L.; Steventon, V.; Furley, A.; Cadby, A. J. *Opt. Commun.* **2017**, *404*, 18−22.
(26) Clemments, A. M.; Botella, P.; Landry, C. C. *J. Am. Chem. Soc.* **2017**, *139*, 3978−3981.
(27) Leduc, C.; Salles, A.; Shorte, S. L.; Etienne-Manneville, S. *J. Visualized Exp.* **2018**, *133*, 1−12.
(28) Sengupta, P.; van Engelenburg, S. B.; Lippincott-Schwartz, J. *Chem. Rev.* **2014**, *114*, 3189−3202.
(29) Aloi, A.; Vargas-Jentzsch, A.; Vilanova, N.; Albertazzi, L.; Meijer, E. W.; Voets, I. K. *J. Am. Chem. Soc.* **2016**, *138*, 2953−2956.
(30) Heilemann, M.; van de Linde, S.; Schüttpelz, M.; Kasper, R.; Seefeldt, B.; Mukherjee, A.; Tinnefeld, P.; Sauer, M. *Angew. Chem., Int. Ed.* **2008**, *47*, 6172−6176.
(31) Baddeley, D.; Bewersdorf, J. *Annu. Rev. Biochem.* **2018**, *87*, 965−989.
(32) Szymborska, A.; de Marco, A.; Daigle, N.; Cordes, V. C.; Briggs, J. A.; Ellenberg, J. *Science* **2013**, *341*, 655−658.
(33) Xia, Y.; Fu, B. M. *Yale J. Biol. Med.* **2018**, *91*, 257−266.
(34) Specht, C. G.; Izeddin, I.; Rodriguez, P. C.; El Beheiry, M.; Rostaing, P.; Darzacq, X.; Dahan, M.; Triller, A. *Neuron* **2013**, *79*, 308−321.
(35) Fernandez, A.; Bautista, M.; Stanciauskas, R.; Chung, T.; Pinaud, F. *ACS Appl. Mater. Interfaces* **2017**, *9*, 27575−27586.
(36) Yan, J.; Zhao, L. X.; Li, C.; Hu, Z.; Zhang, G. F.; Chen, Z. Q.; Chen, T.; Huang, Z. L.; Zhu, J.; Zhu, M. Q. *J. Am. Chem. Soc.* **2015**, *137*, 2436−2439.
(37) Fu, M.; Wang, A.; Zhang, X.; Dai, L.; Li, J. *Angew. Chem.* **2016**, *128*, 920−923.
(38) Wong, R. C.; Ng, D. K.; Fong, W.-P.; Lo, P.-C. *Chem. - Eur. J.* **2017**, *23*, 16505−16515.
(39) Shao, D.; Li, M.; Wang, Z.; Zheng, X.; Lao, Y.-H.; Chang, Z.; Zhang, F.; Lu, M.; Yue, J.; Hu, H.; Yan, H.; Chen, L.; Dong, W.-F.; Leong, K. W. *Adv. Mater.* **2018**, *30*, 1870209.
(40) Lee, B.-Y.; Li, Z.; Clemens, D. L.; Dillon, B. J.; Hwang, A. A.; Zink, J. I.; Horwitz, M. A. *Small* **2016**, *12*, 3690−3702.
(41) Dehghani, S.; Danesh, N. M.; Ramezani, M.; Alibolandi, M.; Lavaee, P.; Nejabat, M.; Abnous, K.; Taghdisi, S. M. *Anal. Chim. Acta* **2018**, *1030*, 142−147.
(42) Adegoke, O.; Seo, M.-W.; Kato, T.; Kawahito, S.; Park, E. Y. *Biosens. Bioelectron.* **2016**, *86*, 135−142.
(43) Niu, D.; Liu, Z.; Li, Y.; Luo, X.; Zhang, J.; Gong, J.; Shi, J. *Adv. Mater.* **2014**, *26*, 4947−4953.
(44) Zhao, S.; Xu, M.; Cao, C.; Yu, Q.; Zhou, Y.; Liu, J. *J. Mater. Chem. B* **2017**, *5*, 6908−6919.
(45) Li, X.; He, Q.; Shi, J. *ACS Nano* **2014**, *8*, 1309−1320.
(46) Gomes, M. C.; Fernandes, R.; Cunha, Â.; Tomé, J. P. *J. Mater. Chem. B* **2013**, *1*, 5429−5435.
(47) Wang, J.; Liu, H.; Leng, F.; Zheng, L.; Yang, J.; Wang, W.; Huang, C. Z. *Microporous Mesoporous Mater.* **2014**, *186*, 187−193.
(48) Olivier, N.; Keller, D.; Gönczy, P.; Manley, S. *PLoS One* **2013**, *8*, No. e69004.
(49) Quan, T.; Li, P.; Long, F.; Zeng, S.; Luo, Q.; Hedde, P. N.; Nienhaus, G. U.; Huang, Z. L. *Opt. Express* **2010**, *18*, 11867−11876.

DOI: 10.1021/acs.analchem.8b05919
Anal. Chem. 2019, 91, 5747−5752